INT. J. NUM. METH. HEAT FLUID FLOW, VOL. 3, 445–456 (1993)

ANALYSIS OF NATURAL CONVECTION MELTING OF A VERTICAL ICE CYLINDER INVOLVING DENSITY ANOMALY

YONGKE WU

Département des Sciences Appliquées, Université du Québec à Chicoutimi, Chicoutimi, Québec G7H 2B1, Canada

AND

MARCEL LACROIX

Département de Génie Mécanique, Université de Sherbrooke, Sherbrooke, Québec J1K 2R1, Canada

ABSTRACT

A numerical study is reported of natural convection melting of ice within a vertical cylinder. A stream function–vorticity–temperature formulation is employed in conjunction with body-fitted coordinates for tracking the irregular shape of the timewise varying solid–liquid interface. A parabolic density profile *versus* temperature is assumed for water. Numerical experiments are carried out for a temperature of the cylinder wall ranging from 4°C to 10°C. Results show that natural convection heat transfer involving density anomaly leads to complex flow patterns and strongly affects the time evolution of the phase front. The maximum Nusselt number at the heated cylinder wall is obtained for $T_w = 4$°C while the minimum is observed for $T_w = 8$°C.

KEY WORDS Ice melting Natural convection

NOMENCLATURE

a_n	coefficient of thermal expansion,
A	aspect ratio, H/r_0,
c_p	specific heat,
F_o	Fourier number $\alpha t/r_0^2$,
g	acceleration of gravity,
g^{11}	$\xi_r^2 + \xi_z^2$,
g^{12}	$\xi_r\eta_r + \xi_z\eta_z$,
g^{22}	$\eta_r^2 + \eta_z^2$,
h	latent heat,
H	height of cylinder,
J^{-1}	$\xi_r\eta_z - \xi_r\eta_z$,
k	thermal conductivity,
n	normal coordinate to the interface,
N	order of thermal expansion $N = 2$,
Nu	Nusselt number, $q/(Hk\Delta T)$,
p	pressure,
P	grids control function, $\nabla^2\xi$,
Pr	Prandtl number, ν/α,
q	heat transfer rate at the heated wall,
Q	grids control function, $\nabla^2\eta$
Ra_1	Rayleigh number defined by (15),
Ra_2	Rayleigh number defined by (16),
r	radial coordinate,
r_0	radius of the ice cylinder,
R	radius in dimensionless form, r/r_0,
Ste	Stefan number, $c_p(T_w - T_f)/h$,
t	time,
T	temperature,
u, v	radial aud axial velocities,
U, V	dimensionless velocities,

0961–5539/93/050445–12$2.00

Received September 1992
Revised April 1993

$\tilde{U}$, $\tilde{V}$ contravariant velocities,
V_f molten fraction,
z axial coordinate,
Z dimensionless axial coordinate, z/r_0

Greek letters

α thermal diffusivity, $k/\rho c_p$,
β thermal expansion coefficient,
ξ, η coordinate in transformed plane,
ξ_r r_η/J,
ξ_z $-r_\eta/J$,
η_r $-z_\xi/J$,
η_z r_ξ/J,
ξ_τ $\xi_r r_\tau + \xi_z z_\tau$,
η_τ $\eta_r r_\tau + \eta_z z_\tau$,
θ dimensionless temperature, $(T - T_f)/(T_w - T_f)$,
ν kinematic viscosity,
ρ density of water,
τ dimensionless time $Ste \cdot Fo$,
ψ stream function,
ω vorticity $\frac{\partial v}{\partial r} - \frac{\partial u}{\partial z}$,
∇^2 Laplacian in non-dimensional cylindrical coordinates,
$\bar{\nabla}^2$ transformed Laplacian.

Subscripts

f fusion,
m maximum density of water,
r reference point,
w cylinder wall.

INTRODUCTION

In recent years, the problem of ice melting has received increasing research attention. The interest for this problem lies in its numerous naturally occurring and technology processes.

It is well known that natural convection plays a significant role during the melting process. Natural convection increases the heat transfer rate and therefore the melting rate and affects the shape and the motion of the solid–liquid interface. For most phase change materials (PCMs), the density of the melt varies linearly with temperature. Hotter fluid is lighter while colder fluid is heavier. Unlike these normal fluids, pure water exhibits, however, an eccentric behaviour, namely the non-linear variation of its density with temperature. The effect of the density anomaly of water at about 4°C on natural convection is of special interest. Flow reversal may occur in the melt region and there may exist a minimum heat transfer rate. Tkachev[1] appears to be the first worker to have noticed this peculiar nature of the maximum density boundary layer. By using photographic techniques, he found a minimum Nusselt number for melting of an ice cylinder at $T_w = 5.5$°C. On the other hand, Saitoh[2] conducted theoretical and experimental work with a horizontal ice cylinder immersed in water. He found that the Nusselt number reaches a minimum value when the wall temperature was about 6.0°C. While studying the same problem in full three-dimensions, Saitoh and Hirose[3] observed an instability in the flow for a wall temperature ranging from 5.5°C to 6.5°C.

A theoretical study performed by Merk[4] predicted a minimum Nusselt number for the melting of a sphere at $T_w = 5.31$°C. These predictions are supported by the experimental work of Dumore *et al.*[5]. A similar study carried out by Vanier *et al.*[6] yielded a minimum Nusselt number at $T_w = 5.35$°C.

Herman *et al.*[7] studied experimentally the influence of density inversion on the melting of ice around a horizontal heated cylinder. They reported a critical condition of the melting process at $T_w = 8$°C. For $T_w > 8$°C natural convection occurs mainly in the upper region of the melt while for $T_w < 8$°C, melting occurs in the lower part. Ho and Chen[8] studied the same case numerically. They found that the minimum heat transfer rate does not always occur for $T_w = 8$°C which is contrary to the results obtained by Herrmann. Heat transfer during melting of ice confined within a heated horizontal cylinder was studied experimentally and theoretically by Rieger *et al.*[9]. Two inner diameters of the cylinder were considered. For both radii, heat transfer reached a minimum value at about $T_w = 8$°C.

In the present study, a numerical analysis is reported for natural convection dominated melting of a vertical ice cylinder involving density anomaly. The computational methodology is first presented and then simulations are carried out for a temperature of the cylinder wall ranging from 4°C to 10°C. Emphasis is placed on the influence of the density anomaly upon phase-change on the convective flow patterns and on the time evolution of the solid–liquid interface.

GOVERNING EQUATIONS

The PCM, i.e., ice, is contained in a cylindrical enclosure of height H and radius r_0. The PCM is assumed to be initially at its fusion temperature T_f, thus eliminating the need for solution of the energy equation in the solid. At time $t = 0$, the surface temperature of the cylinder wall is raised impulsively to a prescribed temperature above the fusion point $T_w > T_f$. The upper and lower walls of the cylinder are adiabatic. As a result, inward melting is triggered. As melting proceeds, the melt layer becomes thicker and natural convection sets in. A schematic of the physical problem is depicted in *Figure 1*.

It is assumed that the thermophysical properties are constant. The Boussinesq approximation is invoked, i.e., liquid density variations arise only in the buoyancy source term, but are otherwise neglected. The liquid is Newtonian and incompressible and the flow is two-dimensional and symmetrical about the vertical centred axis. Volume changes and viscous dissipation are negligible.

Upon the foregoing assumptions, the partial differential equations governing the transport of mass, momentum and energy are:

Continuity equation:

$$\frac{\partial(ru)}{\partial r} + \frac{\partial(rv)}{\partial z} = 0 \tag{1}$$

Momentum equations:

$$\frac{\partial u}{\partial t} + u\frac{\partial u}{\partial r} + v\frac{\partial u}{\partial z} = -\frac{1}{\rho}\frac{\partial p}{\partial r} + \nu\left(\frac{\partial^2 u}{\partial r^2} + \frac{1}{r}\frac{\partial u}{\partial r} + \frac{\partial u^2}{\partial z^2} - \frac{u}{r^2}\right) \tag{2}$$

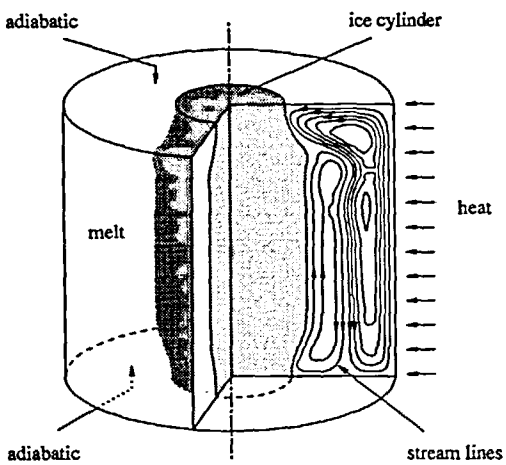

Figure 1 Schematic representation of the physical problem

$$\frac{\partial v}{\partial t} + u\frac{\partial v}{\partial r} + v\frac{\partial v}{\partial z} = -\frac{1}{\rho}\frac{\partial p}{\partial z} + \nu\left(\frac{\partial^2 v}{\partial r^2} + \frac{1}{r}\frac{\partial v}{\partial r} + \frac{\partial^2 v}{\partial z^2}\right) + g\sum_{n=1}^{N} a_n\beta_n(T - T_f)^n \tag{3}$$

Energy equation:

$$\frac{\partial T}{\partial t} + u\frac{\partial T}{\partial r} + v\frac{\partial T}{\partial z} = \alpha\left(\frac{\partial^2 T}{\partial r^2} + \frac{1}{r}\frac{\partial T}{\partial r} + \frac{\partial^2 T}{\partial z^2}\right) \tag{4}$$

Furthermore, since no heat conduction occurs in the solid phase, all heat transferred to the ice–water interface is utilized for melting. Then an energy balance for the interface yields the following condition for the moving boundary:

$$-k\frac{\partial T}{\partial n} = \rho h\frac{\partial n}{\partial t} \tag{5}$$

where n is a normal coordinate to the phase interface.

Since pressure is not a variable of interest in the present study and also to reduce the number of equations, the continuity and momentum equations are reformulated in terms of a stream function ψ and vorticity ω defined as:

$$u = \frac{1}{r}\frac{\partial \psi}{\partial z} \tag{6}$$

$$v = -\frac{1}{r}\frac{\partial \psi}{\partial r} \tag{7}$$

$$\omega = \frac{\partial v}{\partial r} - \frac{\partial u}{\partial z} \tag{8}$$

Taking the curl of the momentum equations (2)–(3) to eliminate pressure and introducing a length scale r_0, a time scale r_0^2/α and a temperature scale $(T_w - T_f)$, the dimensionless governing equations become:

Vorticity:

$$Ste\frac{\partial \omega}{\partial \tau} + \frac{\partial(U\omega)}{\partial R} + \frac{\partial(V\omega)}{\partial Z} = Pr\left(\nabla^2\omega - \frac{\omega}{R}\right) + Pr\sum_{n=1}^{N} a_n\beta_n(Ra)_n\frac{\partial \theta^n}{\partial R} \tag{9}$$

Stream function:

$$\nabla^2\psi = \frac{2}{R}\frac{\partial \psi}{\partial R} - R\omega \tag{10}$$

Energy equation:

$$Ste\frac{\partial \theta}{\partial \tau} + U\frac{\partial \theta}{\partial R} + V\frac{\partial \theta}{\partial Z} = \nabla^2\theta \tag{11}$$

Interface energy equation:

$$-\frac{\partial \theta}{\partial n} = \frac{\partial n}{\partial \tau} \tag{12}$$

The coordinate n is non-dimensional.

The source term in the vorticity transport equation is non-linear due to the nature of density of water. a_n and β_n are coefficients of the non-linear expansion, which are defined in the following section.

INVERSION PARAMETER

To describe the non-linear variation of the density of water with temperature, an approximate relation for the range of 0°C to 20°C is invoked[10]:

$$\rho = \rho_m[1 - \beta(T - T_m)^2] \tag{13}$$

Introducing some reference variable with subscript r, this relation becomes:

$$\rho = \rho_r[1 - 2\beta_1(T - T_r) - \beta_2(T - T_r)^2] \tag{14}$$

where

$$\rho_r = \rho_m[1 - \beta(T_r - T_m)^2]$$
$$\beta_1 = \beta_2(T_r - T_m)$$
$$\beta_2 = \beta/[1 - \beta(T_r - T_m)^2]$$

To define an inversion parameter, two Rayleigh numbers are introduced:

$$(Ra)_1 = \frac{g\beta_1 r_0^3(T_w - T_r)}{\alpha\nu} \tag{15}$$

$$(Ra)_2 = \frac{g\beta_2 r_0^3(T_w - T_r)^2}{\alpha\nu} \tag{16}$$

Then, an inversion parameter is defined as:

$$\gamma = \frac{(Ra)_1}{(Ra)_2} = -\frac{T_m - T_r}{T_w - T_r} = -\theta_m \tag{17}$$

Substituting this inversion parameter into (9), the non-linear source term becomes:

$$Pr \sum_{n=1}^{2} a_n\beta_n(Ra)_n \frac{\partial\theta^n}{\partial R} = 2Pr(Ra)_2(\gamma + \theta)\frac{\partial\theta}{\partial R} \tag{18}$$

Hereafter, we shall use γ and $(Ra)_2$ instead of $(Ra)_1$ and $(Ra)_2$ and the subscript 2 will be omitted for the sake of clarity.

It is worth noticing that if γ is positive, the source term will act qualitatively as in a normal fluid. If γ is negative, it can reduce and even cancel out the buoyancy force. By choosing a reference temperature $T_r = T_f = 0$, the range of γ is confined to $-\infty < \gamma < 0$. Since θ is defined as $0 \leqslant \theta \leqslant 1$, the source term becomes negative for $\gamma < -1$, leading to a buoyancy force in an opposite direction to that of a normal fluid. For $-1 < \gamma < 0$, the source term can be either positive or negative depending on the dimensionless temperature θ within the melt region. Thus, two counter-rotating vortices can appear within the melt region at the same time, corresponding to the phenomenon of flow reversal.

TRANSFORMED EQUATIONS

As melting proceeds, the phase front moves inward while being distorted by the non-uniform heat fluxes along its surface. As a result, the shape of the solid–liquid interface will not coincide, in general, with the grid nodes of a cylindrical grid. It is then difficult to implement the discretized boundary conditions and attempts to solve the resulting finite-difference equations may fail to yield accurate and convergent solutions.

To overcome these difficulties, body-fitted coordinates are considered. The conservation equations (9)–(12) are cast from the original cylindrical grid (R, Z) to a curvilinear grid (ξ, η). The resulting equations are more complicated but their boundary conditions are now specified

on straight boundaries and the computational grid is rectangular and uniformly spaced. Performing this transformation, (9)–(11) become in the (ξ, η) grid:

$$Ste\frac{\partial\omega}{\partial\tau} + \tilde{U}\frac{\partial\omega}{\partial\xi} + \tilde{V}\frac{\partial\omega}{\partial\eta} = Pr\tilde{\nabla}\omega + S_\omega \tag{19}$$

$$\tilde{\nabla}^2\psi = S_\psi \tag{20}$$

$$Ste\frac{\partial\theta}{\partial\tau} + \tilde{U}\frac{\partial\theta}{\partial\xi} + \tilde{V}\frac{\partial\theta}{\partial\eta} = \tilde{\nabla}^2\theta + S_\theta \tag{21}$$

where $\tilde{U}$ and $\tilde{V}$ are contravariant velocities expressed by:

$$\tilde{U} = \xi_r U + \xi_z V \tag{22}$$

$$\tilde{V} = \eta_r U + \eta_z V \tag{23}$$

and

$$\begin{aligned}
U &= \frac{1}{R}\left(\xi_z\frac{\partial\psi}{\partial\xi} + \eta_z\frac{\partial\psi}{\partial\eta}\right)\\
V &= -\frac{1}{R}\left(\xi_r\frac{\partial\psi}{\partial\xi} + \eta_r\frac{\partial\psi}{\partial\eta}\right)\\
S_\omega &= Ste\left(\xi_\tau\frac{\partial\omega}{\partial\xi} + \eta_\tau\frac{\partial\omega}{\partial\eta}\right) + \left(\frac{U}{R} - \frac{Pr}{R^2}\right)\omega + 2PrRa(\gamma+\theta)\left(\xi_r\frac{\partial\theta}{\partial\xi} + \eta_r\frac{\partial\theta}{\partial\eta}\right)\\
S_\psi &= \frac{2}{R}\left(\xi_r\frac{\partial\psi}{\partial\xi} + \eta_r\frac{\partial\psi}{\partial\eta}\right) - R\omega\\
S_\theta &= Ste\left(\xi_\tau\frac{\partial\theta}{\partial\xi} + \eta_\tau\frac{\partial\theta}{\partial\eta}\right)\\
\tilde{\nabla}^2 &= g^{11}\frac{\partial^2}{\partial\xi^2} + 2g^{12}\frac{\partial^2}{\partial\xi\eta} + g^{22}\frac{\partial^2}{\partial\eta^2} + P\frac{\partial}{\partial\xi} + Q\frac{\partial}{\partial\eta} + \frac{1}{R}\left(\xi_r\frac{\partial}{\partial\xi} + \eta_r\frac{\partial}{\partial\eta}\right)
\end{aligned} \tag{24}$$

$\tilde{\nabla}^2$ is the transformed Laplacian operator in cylindrical coordinates.

The energy balance equation (12) is transformed and alternatively split into components as:

$$\frac{\partial R}{\partial\tau} = -\frac{\partial\theta}{\partial\xi}\xi_r \tag{25}$$

$$\frac{\partial Z}{\partial\tau} = -\frac{\partial\theta}{\partial\xi}\xi_z \tag{26}$$

To find the liquid–solid interface position, the above equations have to be integrated as a function of time.

The boundary conditions in the computational space are:

$\xi = \xi_{\min}$,	$\xi = \xi_{\max}$
$U = 0$	$U = 0$
$V = 0$	$V = 0$
$\theta = 0$	$\theta = 1$
$\psi = 0$	$\psi = 0$
$\omega = \xi_r V_\xi - \xi_z U_\xi$	$\omega = \xi_r V_\xi - \xi_z U_\xi$

$$\eta = \eta_{\min} \quad \text{and} \quad \eta = \eta_{\max},$$
$$U = 0$$
$$V = 0$$
$$\psi = 0$$
$$\omega = \eta_r V_\eta - \eta_z U_\eta$$
$$g^{22}\theta_\eta + g^{12}\theta_\xi = 0$$

NUMERICAL PROCEDURE

The governing equations (19)–(21) and (25)–(26) with the corresponding boundary conditions are solved numerically with a finite-difference method. A first order forward difference approximation is used for the time derivatives. The diffusion terms are replaced by second-order central difference approximations. Special attention is paid, however, to the convection terms. It is well known that the use of second-order central difference approximations for these terms may produce unstable and divergent solutions for high Peclet cell numbers (or high Rayleigh numbers)[11]. Although the use of a first-order upwind scheme may eliminate these wiggly solutions, it introduces truncation errors and produces significant artificial diffusion. In the present study, this problem is overcome by adopting a second-order upwind scheme.

The proposed scheme has the following form:

$$u\frac{\partial f}{\partial \xi} = A^u f_{i-2} + B^u f_{i-1} + C^u f_i + D^u f_{i+1} + E^u f_{i+2} \tag{27}$$

where A^u, B^u, C^u, D^u and E^u are functions of u. These coefficients are defined in the Appendix. The resulting finite-difference scheme for the vorticity (19) and temperature equations (21) has the form:

$$a_1 f_{i-2,j} + a_2 f_{i-1,j} + a_3 f_{i+1,j} + a_4 f_{i+2,j} + a_5 f_{i,j-2} + a_6 f_{i,j-1} + a_7 f_{i,j+1} + a_8 f_{i,j+2} + a_9 f_{i+1,j+1} + a_{10} f_{i+1,j-1} + a_{11} f_{i-1,j-1} + a_{12} f_{i-1,j+1} + a_{13} f_{i,j} = S \tag{28}$$

Expressions for the coefficients in (28) may be found in Reference 11. This finite-difference equation is solved by means of an alternating penta-diagonal matrix algorithm[11]. For the stream function (20), only second-order finite differences are used and the resulting discretized equation is solved by a tridiagonal matrix algorithm.

The overall calculation procedure consists of the following steps:

1. Set initial values of all the variables $U_{i,j}$, $V_{i,j}$, $\omega_{i,j}$ and $\psi_{i,j}$ to zero. The initial temperatures are set to zero everywhere in the field except for the nodes at the heated boundary which are put equal to 1.
2. Set the initial boundary grid nodes for the physical domain.
3. Generate a new grid for the physical domain.
4. Calculate all geometric coefficients for the transformed equations.
5. Compute $\omega_{i,j}$ with the current values of $U_{i,j}$, $V_{i,j}$, $\psi_{i,j}$ and $\theta_{i,j}$.
6. Compute $\psi_{i,j}$ with the updated values $\omega_{i,j}$.
7. Compute $U_{i,j}$, $V_{i,j}$ with the updated values $\psi_{i,j}$ and velocity boundary conditions.
8. Compute $\theta_{i,j}$ with the updated values $U_{i,j}$ and $V_{i,j}$.
9. Check for convergence. If satisfied, go to the next step; otherwise, go back to step 5.

10. Check for time to stop. If positive, stop; otherwise, go to the next step.
11. Update x_0, y_0, ω_0 and θ_0 for the next time step.
12. Calculate the new interface position.
13. Perform a rezoning procedure.
14. Go back to step 3 to begin computations for the next time step.

Steps 3, 9 and 13 need further explanations. In step 3, a new grid is generated from the numerical solution of a set of two coupled non-linear elliptic partial differential equations for the cylindrical coordinates as a function of the curvilinear coordinates. This procedure is commonly used for mapping complex geometries and details concerning its implementation may be found in Reference 11.

In step 9, convergence is declared when:

$$\sum_{i}^{N}\sum_{j}^{N} \|R\| \leqslant 10^{-4} \tag{29}$$

where $\|R\|$ is the residual for the continuity equation and when:

$$\|f_{i,j}^{k+1} - f_{i,j}^{k}\| \leqslant 10^{-4} \tag{30}$$

where f denotes the vorticity and temperature and k denotes the iteration number.

According to the energy balance equation (5), the local velocity of the interface should be locally orthogonal to the interface. Generally, the melting is non-uniform along the interface because of natural convection. Therefore, the interface can become curved as the boundary is moving. If the interface becomes locally convex, the moving interface grid points have a tendency to move towards their reflex centre. As melting proceeds, the generated grids can be distorted and eventually the grid nodes may overlap. To overcome these difficulties, an implicit rezoning procedure is employed in step 13. Once the interface is determined at time level, $\tau + \Delta\tau$, a spline interpolation procedure is used to redistribute the boundary grid points at equal arc length intervals along the interface. Thereby, a proper grid network system is available for carrying out the calculations at time $\tau + \Delta\tau$. Further details on this rezoning procedure are given in Reference 11.

RESULTS AND DISCUSSION

The foregoing computational methodology has been thoroughly tested for natural convection dominated melting around a vertical heated cylinder and within a vertical cylinder heated from below. The numerical predictions were testified against other numerical solutions and experimental data[11].

To avoid computational difficulties at time $\tau = 0$, a very thin uniform thickness melt layer parallel to the heated wall was assumed to exist initially. The layer thickness was chosen such that the Rayleigh number based on this initial gap width was small enough so that pure conduction could be considered as the prevailing mechanism of heat transfer.

Following a grid refinement study and as a compromise between cost and accuracy, the calculations presented here were done with a grid size of 11×31 non-uniformly distributed nodes. This makes it possible to concentrate several grid points in the critical regions near the heated surface and near the solid–liquid interface where large temperature and vorticity gradients prevail. A constant time step of 10^{-3} was utilized in order to assure small interface motion from one time step to the next. No attempts were made to optimize (increase) the time step as melting proceeds.

All the simulations presented here were carried out for a cylindrical enclosure with an aspect ratio $A = 2.0$ and for isothermal boundary conditions T_w ranging from 4°C to 10°C. The Rayleigh number was kept constant at 7×10^5. The inversion parameter γ, the Prandtl number Pr and the Stefan number Ste are summarized in *Table 1*.

Table I Summary of the test cases

Parameter	$T_w = 4°C$	$T_w = 6°C$	$T_w = 8°C$	$T_w = 10°C$
γ	−1.0	−0.667	−0.5	−0.4
Pr	11.5	10.55	10.0	9.4
Ste	0.05	0.075	0.10	0.125

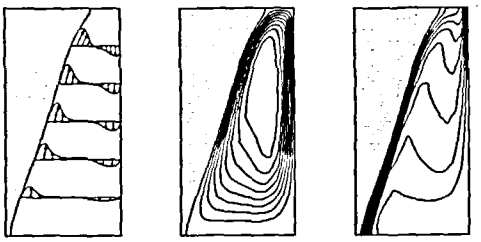

Figure 2 Velocity field, streamlines and isotherms for $T_w = 4°C$ and at $\tau = 0.06$

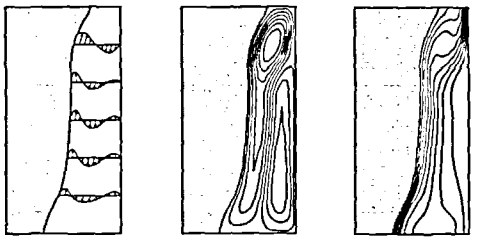

Figure 3 Velocity field, streamlines and isotherms for $T_w = 6°C$ and at $\tau = 0.06$

At early times, the melting scenario is the same for all cases. Heat transfer in the melt zone is predominated by conduction (the isotherms remain vertical) and the ice–water interface moves parallel to the heated cylinder wall. The solid–liquid interface being an isotherm itself, always intersects the adiabatic top and bottom boundaries at right angles. After a while, the thickness of the melt layer becomes large enough so that natural convection is triggered. As time passes, the melt layer expands and natural convection becomes the prevailing mechanism of heat transfer inside the melt. The intensity and the direction of the buoyancy driven flows are dependent on the boundary condition for the wall temperature. As a result, the local heat transfer rates along the solid–liquid interface are strongly perturbed and so are the movement and the shape of the phase front.

Figure 2 displays the vertical velocity profiles, the streamlines and the isotherms at time $\tau = 0.06$ and for the case with $T_w = 4°C$. The increments between streamlines and isotherms are constant ranging from their minimum value to their maximum value respectively. This Figure depicts a unicellular flow pattern with a larger melt region in the lower part of the cylinder. High melting occurs at the bottom of the solid–liquid interface where warm and denser fluid impinges after being heated by the hot wall. As the fluid ascends along the interface, heat is transferred to the melting front and the liquid becomes cooler and lighter. Consequently, the melting rate at the bottom is significantly larger than that at the top. This recirculation behaviour is just the opposite to that normally observed in most fluids.

For the case with $T_w = 6°C$, a dual cell flow pattern occurs (*Figure 3*). As water with maximum density is located somewhere in the melt region, two counterrotating recirculation bubbles have established themselves at time $\tau = 0.06$. Since the point of maximum density (taking place at $T = 4°C$) is closer to the cylinder than to the interface, the inner recirculating eddy is stronger than the outer one. As a result, melting near the bottom is still faster than that near the top of the cylinder.

When the surface temperature of the cylinder is further increased to $T_w = 8°C$, the point of maximum water density is located in the vertical plane midway between the cylinder surface and the phase front. Consequently, in the early stages of melting, the strength of both the inner and outer eddies is nearly the same and the phase front moves parallel to the cylinder wall (*Figure 4*). As melting progresses, the counterrotating eddies increase in size and high melting

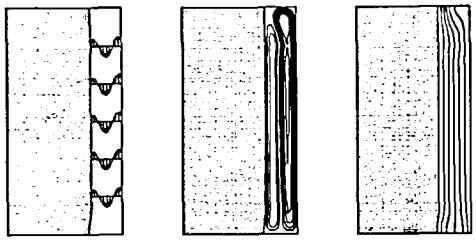

Figure 4 Velocity field, streamlines and isotherms for $T_w = 8°C$ and at $\tau = 0.03$

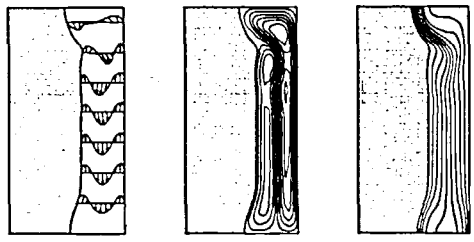

Figure 5 Velocity field, streamlines and isotherms for $T_w = 8°C$ and at $\tau = 0.70$

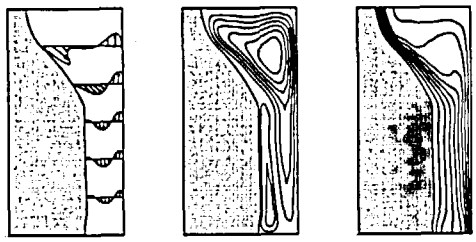

Figure 6 Velocity field, streamlines and isotherms for $T_w = 10°C$ and at $\tau = 0.06$

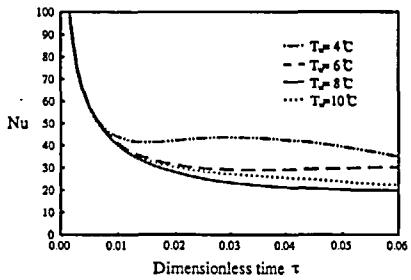

Figure 7 Temporal variation of the average Nusselt number at the heated wall

occurs at the top and at the bottom of the solid–liquid interface (*Figure 5*). The local temperature gradients are clearly higher near the top and the bottom of the phase front, accounting for the higher melt front velocity there.

For the case with $T_w = 10°C$, the region of maximum water density is displaced towards the interface and the outer recirculation bubble grows stronger than the inner one (*Figure 6*). The resulting flow pattern bears many resemblances with that for a normal fluid except for the presence of a weak counterrotating eddy near the bottom of the phase font.

The timewise variations of the average Nusselt number at the heated wall are depicted in *Figure 7*. These Nusselt numbers were calculated from the converged temperature field at each time step. The results display a rapid decrease in the heat transfer rate at the early stages of melting. This behaviour results from transient heat conduction. As soon as natural convection sets in the melt, the heat transfer rate starts increasing. This is clearly shown for the case with $T_w = 4°C$ and, to a lesser extent, for the case with $T_w = 6°C$. In both these cases, a strong clockwise recirculating eddy establishes itself along the phase front yielding large temperature gradients and therefore enhanced heat transfer rates. For the cases with $T_w = 8°C$ and $T_w = 10°C$, counterrotating eddies prevail in the melt and the heat transfer rates continue to decrease monotonically.

The effect of the flow pattern on the temporal variation of the molten volume fraction is depicted in *Figure 8*. The melting rate is maximum for $T_w = 4°C$ and minimum for $T_w = 8°C$. Also, this fraction increases almost linearly with time once the convective motion is well established throughout the melt.

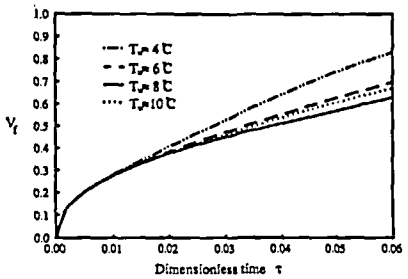

Figure 8 Temporal variation of the molten volume fraction

CONCLUDING REMARKS

A numerical study of natural convection dominated melting of ice within a vertical heated cylinder enclosure has been conducted. The study focused on the density anomaly upon melting via natural convection. A robust computational methodology based on body-fitted coordinates was adopted for handling the complex motion and irregular shape of the time-varying solid–liquid interface. Results have shown that the convective flow patterns, the heat transfer rates and the time evolution of the phase front are strongly affected by the inversion density. A unicellular flow pattern, occurring at $T_w = 4°C$, yields maximum heat transfer and melting rates while multicellular flow patterns, taking place at $T_w = 8°C$, yield minimum heat transfer and melting rates.

ACKNOWLEDGEMENT

The authors are very grateful to the National Science and Engineering Research Council of Canada for their financial support.

REFERENCES

1 Tkachev, A. G. Heat exchange in melting and freezing of ice, *Problems of Heat Transfer during a Change of State, AEC-TR 3405*, pp. 169–178 (1953)
2 Saitoh, T. Numerical method for multidimensional freezing problems in arbitrary domains, *J. Heat Transfer*, **100**, 294–299 (1978)
3 Saitoh, T. and Hirose, K. High Rayleigh number solutions to problem of latent heat thermal energy storage in a horizontal cylinder capsule, *J. Heat Transfer*, **104**, 545–553 (1982)
4 Merk, H. J. The influence of melting and anomalous expansion on the thermal convection in laminar boundary layers, *Appl. Sci. Res.*, **4**, 435–452 (1954)
5 Dumore, J. M., Merk, H. J. and Prins, J. A. Heat transfer from water to ice by thermal convection, *Nature*, **172**, 460–461 (1953)
6 Vanier, C. R. and Tien, C. Effect of maximum density and melting on natural convection heat transfer from a vertical plate, *Chem. Eng. Progr. Symp. Ser.*, **64**, 240–254 (1968)
7 Herman, J., Leindenfrost, W. and Viskanta, R. Melting of ice around a horizontal isothermal cylindrical heat source, *Chem. Eng. Commun.*, **25**, 63–78 (1984)
8 Ho, C. J. and Chen, S. Numerical simulation of melting of ice around a horizontal cylinder, *Int. J. Heat Mass Transfer*, **29**, 1359–1369 (1986)
9 Rieger, H., Projahn, U., Bereiss, M. and Beer, H. Heat transfer during melting inside horizontal tube, *J. Heat Transfer*, **105**, 226–234 (1983)
10 Nguyen, T. H., Vasseur, P. and Robillard, L. Natural convection between horizontal concentric cylinders with density inversion of water for low Rayleigh number, *Int. J. Heat Mass Transfer*, **25**, 1559–1568 (1982)
11 Wu, Y. K. Numerical studies of melting process in a cylindrical enclosure, *PhD Thesis* (1990)

APPENDIX

Coefficients in (27) are:

$$A^u = \frac{|u| + u}{4\Delta\xi}$$

$$B^u = \frac{|u| + u}{\Delta\xi}$$

$$C^u = \frac{3|u|}{2\Delta\xi} \tag{31}$$

$$D^u = -\frac{|u| - u}{\Delta\xi}$$

$$E^u = \frac{|u| - u}{4\Delta\xi}$$